MHD Chemically Reacting and Radiating Nanofluid Flow over a Vertical Cone Embedded in a Porous Medium with Variable Properties

P.Yogeswara Reddy[1], Dr.G.S.S. Raju[2]

[1.] *Department of Mathematics, Vemana Institute of Technology, Bengaluru, Karnataka, India.*
[2.] *Department of mathematics, JNTU College of Engineering, Pulivendula, YSR(cuddapah) Dist, A.P, India.*

Abstract: **In this study, we examine the combined effects of thermal radiation, chemical reaction on MHD hydromagnetic boundary layer flow over a vertical cone filled with nanofluid saturated porous medium under variable properties. The governing flow, heat and mass transfer equations are transformed into ordinary differential equations using similarity variables and are solved numerically by a Galerkin Finite element method. Numerical results are obtained for dimensionless velocity, temperature, nanoparticle volume fraction, as well as the skin friction, local Nusselt and Sherwood number for the different values of the pertinent parameters entered into the problem. The effects of various controlling parameters on these quantities are investigated. Pertinent results are presented graphically and discussed quantitatively. The present results are compared with existing results and found to be good agreement. It is found that the temperature of the fluid remarkably enhances with the rising values of Brownian motion parameter (*Nb*).**

Keywords: **MHD; Nanofluid; Vertical cone; Variable properties; Chemical reaction; Thermal radiation.**

Nomenclature

k_m	Thermal conductivity
Nu_x	Nusselt number
ϕ	Nanoparticle volume fraction
ϕ_w	Nanoparticle volume fraction on the plate
ϕ_∞	Ambient nanoparticle volume fraction
(x, y)	Cartesian coordinates
T_w	Temperature at the plate
T_∞	Ambient temperature attained
T	Temperature on the plate
Ra_x	Rayleigh number
q_w	Wall heat flux
j_w	Wall mass flux
D_B	Brownian diffusion
D_T	Thermophoretic diffusion coefficient
β_0	Strength of magnetic field
g	Gravitational acceleration vector
Nt	Thermophoresis parameter
Le	Lewis number
P	Pressure
Nb	Brownian motion parameter
q_r	Thermal radiation
M	Magnetic parameter
Sh_x	Local Sherwood number
Nv	Variable viscosity parameter
Nc	Variable thermal conductivity parameter
Cr	Chemical reaction parameter
Nr	Buoyancy ratio
K	Permeability of the porous medium *Greek symbols*
μ	viscosity ε porosity
γ	proportionality constant
α_m	Thermal diffusivity.
ρ_f	Fluid density
ρ_p	Nanoparticle mass density
ψ	Stream function
V	Kinematic viscosity of the fluid
τ	Parameter defined by $\varepsilon \frac{(\rho c)_p}{(\rho c)_f}$
$(\rho c)_f$	Heat capacity of the fluid
Ø (η)	Dimensionless nanoparticle volume fraction
η	Similarity variable
θ (η)	Dimensionless temperature
$(\rho c)_p$	Effective heat capacity of the nanoparticle
α	Acute angle of the plate to the vertical
β	Volumetric expansion coefficient *Subscripts*
w	Condition on the plate
∞	Condition far away from the plate
η	Similarity variable
f	Base fluid

I. INTRODUCTION

In recent years the field of science and technology, nanotechnology has become more popular because of its specific application to the arenas of electronics, fuel cells, space, fuels, better air quality, batteries, solar cells, medicine, cleaner water, chemical sensors and sporting goods. In the understanding of all these features, there is a vital field acknowledged as the nanofluid, which is fundamentally a homogenous mixture of the base fluid and nanoparticles. Nanoparticles are the particles and are of 1-100 nm in size. The convectional heat transfer fluids like water, oil, kerosene and ethylene glycol have poor heat transfer capabilities due to their low thermal conductivity. To improve the thermal conductivity of these fluids nano/micro-sized materials are suspended in liquids. The thermal conductivity of the metals is three times higher than the general fluids, so it is desirable to combine the two substances. Due to the nanofluid thermal enhancement, performance, applications and benefits in several important arenas, the nanofluid has contributed significantly well in the field of microfluidics, manufacturing, microelectronics, advanced nuclear systems, polymer technology, transportation, medical, saving in energy. Choi [1] was the first among all who introduced a new type of fluid called nanofluid while doing research on new coolants and cooling technologies. Eastman et al. [2] have noticed in an experiment that the thermal conductivity of the base fluid (water) has increased up to 60% when CuO nanoparticles of volume fraction 5% are added to the base fluid. This is because of increasing surface area of the base fluid duo to the suspension of nanoparticles. Eastman et al. [3] have also showed that the thermal conductivity has increased 40% when copper nanoparticles of volume fraction less than 1% are added to the ethylene glycol or oil. Xuan et al. [4] have reported that the convective flow and heat transfer characteristics of nanofluids. Buongiorno [5] has reported in experimental study that nanoparticle size, inertia, particle agglomeration, Magnus effect, volume fraction of the nanoparticle, Brownian motion and thermophoresis are the influencing parameters. Nield and Kuznetsov [6] have discussed the Cheng-Mincowycz problem for natural convection boundary-layer flow in a porous medium saturated nanofluid. Kuznetsov and Nield [7] studied the influence of Brownian motion and thermophoresis on natural convection boundary layer flow of a nanofluid past a vertical plate.

Natural convection flow, heat and mass transfer over curved bodies through nanofluid saturated porous medium is an important area in recent years because of its wide range applications such as chemical engineering, thermal energy storage devices, heat exchangers, ground water systems, electronic cooling, boilers, heat loss from piping, nuclear process systems etc. Keeping above applications in mind, several authors, Chamkha et al. [8] analyzed the sway of thermo-diffusion and Diffusion-thermo effects on mixed convection flow of nanofluid over a vertical cone saturated in a porous medium with chemical reaction. Chamkha et al. [9] have discussed the mixed convection flow of nanofluid over vertical cone embedded in porous medium with thermal radiation. Gorla et al. [10] have studied nanofluid natural convection boundary layer flow through porous medium over a vertical cone. Chamkha et al. [11] have investigated Non-Newtonian nanofluid natural convection flow over a cone through porous medium with uniform heat and volume fraction fluxes. Cheng [12] has presented double-diffusive natural convection heat and mass transfer of a porous media saturated nanofluid over a vertical cone. Behseresht et al. [13] discussed heat and mass transfer features of a nanofluid over a vertical cone using practical range of thermo-physical properties of nanofluids. Recently, Ghalambaz et al. [14] have analyzed the influence of nanoparticle diameter and concentration on natural convection heat and mass transfer of Al_2O_3 -water based nanofluids over a vertical cone. The numerical study of hydromagnetic flow of a reactive nanofluid over a stretching surface with or without bioconvection was carried out by Makinde and Animasaun [15, 16] and Makinde et al. [17]. Teamah et al. [18] investigated the effects of heat source on MHD natural convection of nanofluid in square cavity. Sudarsana Reddy et al. [19] have presented natural convection boundary layer heat and mass transfer characteristics of Al_2O_3 - water and Ag - water nanofluids over a vertical cone. Sheremet et al. [20] presented Buongiorno's mathematical model of nanofluid over a square cavity through porous medium. Sheremet et al. [21] have deliberated three-dimensional natural convection Buongiorno's mathematical model of nanofluid over a porous enclosure. Ellahi et al. [22] have reported Non-Newtonian flow, heat transfer between two coaxial cylinders through nanofluid saturated porous medium with variable viscosity. Sheikholeslami et al. [23] have analyzed the natural convection heat transfer in an elliptic inner cylinder filled with nanofluid.

In all the above studies the viscosity and thermal conductivity of nanofluids are taken as constant. That is, dynamic viscosity and thermal conductivity of the nanofluid are considered as constant. It is well known fact that the fluid characteristics may varies with temperature, so, to predict exactly the flow, heat and mass transfer characteristics of the fluid it is necessary to consider the viscosity and thermal conductivity of the fluid as the function of temperature [24, 25]. In the present analysis we have considered working fluid as the nanofluid. The study of existing literature on nanofluids discloses that the nanofluids viscosity and thermal conductivity is to be varies and are strongly varies with temperature [26, 27]. Khanafer and Vafai [28] conducted both theoretical and experimental reviews to analyze the impact of variable viscosity and thermal conductivity of the nanofluids. Kakac and Pramuanjaroenkij [29] have also examined the thermo physical features of nanofluids. Noghrehabadi et al. [30] have reported the boundary layer flow and heat transfer analysis of nanofluid over a vertical cone embedded in porous

medium saturated with nanofluid. Sudarsana Reddy et al. [31] have discussed the effect of variable viscosity and thermal conductivity on heat and mass transfer flow of nanofluid over a stretching sheet. Sudarsana Reddy [32] has discussed MHD natural convection heat transfer enhancement of Cu – water and Ag – water based nanofluid over a rotating disk under the influence of chemical reaction. Aly [33] have perceived the impact of Soret and Dufour effects on natural con2vention of nanofluid over circular cylinder using finite volume method and found that size and formation of cells inside the enclosure are strongly depending on the Rayleigh number. Yan Zhang et al. [34] reported the influence of magnetic field and velocity slip on flow and heat transfer analysis of power – low nanofluid thin film over a stretching sheet. In this study they have considered three types of nanoparticles, Al_2O_3, TiO_2 and CuO with ethylene vinyl acetate copolymer (EVA) as the base fluid and reported that CuO – EVA based nanofluid has better heat transfer enhancement than the Al_2O_3 – EVA and TiO_2 – EVA nanofluid. Dhanai et al. [35] studied flow and heat transfer analysis of non-Newtonian nanofluid by taking heat source/sink and variable magnetic field.

The main aim of this article is to address the influence of variable viscosity and variable thermal conductivity on MHD boundary layer heat and mass transfer flow of nanofluid over a vertical cone embedded in porous medium with thermal radiation and chemical reaction. As a result the parameters (*Nv*) and (*Nc*) are entered into the problem. The problem presented here has immediate applications in biomedical systems, electronic devices, food processing, manufacturing, cooling systems, etc. To our knowledge, the problem is new and no such articles reported yet in the literature.

II. MATHEMATICAL ANALYSIS OF THE PROBLEM

We assume a steady two-dimensional viscous incompressible natural convection nanofluid flow over a vertical cone embedded in porous medium in the presence of variable viscosity and thermal conductivity with the coordinate system given in Fig.1. The fluid is assumed an electrically conducted through a non-uniform magnetic field of strength B_0 applied in the direction normal to the surface of the cone. It is assumed that T_w, and ϕ_w are the temperature and nanoparticle volume fraction at the surface of the cone (y=0) and T_∞ and ϕ_∞ are the temperature and nanoparticle volume fraction of the ambient fluid, respectively. In the present analysis the nanoparticles are persuaded in the base fluid according to the Brownian motion and thermophoresis. Based on the works of Buongiorno [5] and by employing the Oberbeck - Boussinesq approximation the governing equations describing the flow, heat and mass transfer for nanofluids in the presence of thermal radiation and chemical reaction parameters take the following form:

$$\frac{\partial(ru)}{\partial x}+\frac{\partial(rv)}{\partial y}=0 \tag{1}$$

$$\frac{\partial p}{\partial y}=0 \tag{2}$$

$$\frac{\partial v}{\partial x}=-\frac{\mu(T)}{K}u+g\left[(1-\phi_\infty)\rho_{f\infty}\beta(T-T_\infty)-(\rho_p-\rho_{f\infty})(\phi-\phi_\infty)\right]\cos\gamma-\frac{\sigma B_0^2}{\rho_f}u \tag{3}$$

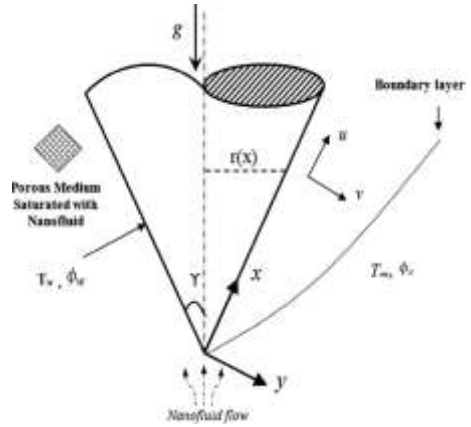

Fig.1. Physical model and coordinate

$$\left(u\frac{\partial T}{\partial x}+v\frac{\partial T}{\partial y}\right)=\frac{1}{(\rho c_p)_{nf}}\frac{\partial}{\partial y}\left(k_m(T)\frac{\partial T}{\partial y}\right)+\frac{(\rho c)_p}{(\rho c_p)_{nf}}\left[D_B\frac{\partial\phi}{\partial y}\cdot\frac{\partial T}{\partial y}+\left(\frac{D_T}{T_\infty}\right)\left(\frac{\partial T}{\partial y}\right)^2\right]-\frac{1}{(\rho c_p)_{nf}}\cdot\frac{\partial}{\partial y}(q_r) \tag{4}$$

$$\frac{1}{\varepsilon}\left(u\frac{\partial\phi}{\partial x}+v\frac{\partial\phi}{\partial y}\right)=D_B\frac{\partial^2\phi}{\partial y^2}+\left(\frac{D_T}{T_\infty}\right)\frac{\partial^2 T}{\partial y^2}-K_r(\phi-\phi_\infty) \tag{5}$$

The corresponding boundary conditions are

$$u=0,\quad T=T_w,\quad \phi=\phi_w \qquad at\quad y=0 \tag{6}$$

$$u\to 0,\quad T\to T_\infty,\quad \phi\to\phi_\infty \qquad at\quad y\to\infty \tag{7}$$

In the present study, the thermal conductivity and viscosity are taken as the function of temperature. Therefore, the viscosity in terms of temperature can be written as follows:

$$\frac{1}{\mu}=\frac{1}{\mu_\infty}\left[1+\gamma(T-T_\infty)\right] \tag{8}$$

The above equation can be simplified as

$$\frac{1}{\mu}=m_\mu(T-T_r) \tag{9}$$

where, m_μ and T_r are can be defined as

$m_\mu=\frac{\gamma}{\mu_\infty}$ and $T_r=T_\infty-\frac{1}{\gamma}$.

In the above equations (8) and (9), μ_∞, m_μ, T_∞, T_r, and γ are constant values.

The thermal conductivity of nanoparticles is defined as

$$k_m(T)=k_\infty\left(1+m_k(T-T_\infty)\right) \tag{10}$$

where, $m_k = \frac{Nc}{(T_w - T_\infty)}$ and Nc is the variable thermal conductivity parameter, k_∞ is the effective thermal conductivity. By using Rosseland approximation for radiation, the radiative heat flux q_r is defined as

$$q_r = -\frac{4\sigma^*}{3K^*}\frac{\partial T^4}{\partial y} \tag{11}$$

where, σ^* is the Stephan-Boltzman constant, K^* is the mean absorption coefficient. We assume that the temperature differences within the flow are such that the term T^4 may be expressed as a linear function of temperature. This is accomplished by expanding T^4 in a Taylor series about the free stream temperature T_∞ as follows:

$$T^4 = T_\infty{}^4 + 4T_\infty{}^3(T - T_\infty) + 6T_\infty{}^2(T - T_\infty)^2 + \cdots \tag{12}$$

Neglecting higher-order terms in the above equation (12) beyond the first degree in $(T - T_\infty)$, we get

$$T^4 \cong 4T_\infty{}^3 T - 3T_\infty{}^4 . \tag{13}$$

Thus, substituting Eq. (13) into Eq. (11), we get

$$q_r = -\frac{16T_\infty{}^3\sigma^*}{3K^*}\frac{\partial T}{\partial y}. \tag{14}$$

The continuity equation (1) is satisfied by introducing a stream function (ψ) as

$$u = \frac{1}{r}\frac{\partial \psi}{\partial y}, \qquad v = -\frac{1}{r}\frac{\partial \psi}{\partial x} \tag{15}$$

The following similarity transformations are introduced to simplify the mathematical analysis of the problem

$$\eta = \frac{y}{x}Ra_x^{1/2}, \; f(\eta) = \frac{\psi}{\alpha_m . r . Ra_x^{1/2}}, \; \theta(\eta) = \frac{T - T_\infty}{T_w - T_\infty}, \; \emptyset(\eta) = \frac{\phi - \phi_\infty}{\phi_w - \phi_\infty}$$
$$, Nv = \frac{T_r - T_\infty}{T_w - T_\infty}, \tag{16}$$

where Ra_x is the local Rayleigh number and is defined as

$$Ra_x = \frac{g\beta K\rho_{f\infty}(1 - \phi_\infty)(T_w - T_\infty)\, x\, Cos\gamma}{\mu_\infty \alpha_m}, \tag{17}$$

and r coordinate is related to the x coordinate by $r = x\, sin\gamma$. Using the similarity variables (16) and making use of Eqs. (14), the governing equations (3) - (5) together with boundary conditions (6) and (7) reduce to

$$\frac{Nv}{(Nv - \emptyset)}f''' + \frac{Nv}{(Nv - \emptyset)^2}f'\emptyset' - (\theta' - Nr\,\emptyset') - Mf' = 0, \tag{18}$$

$$(1 + R)\theta'' + Nc\,\emptyset\,\theta'' + \tfrac{3}{2}f\theta' + Nc\,\theta'\emptyset' + Nt(\theta')^2 + Nb\,\emptyset'\theta' = 0, \tag{19}$$

$$\emptyset'' + \frac{3}{2}Le\, f\,\emptyset' + \frac{Nt}{Nb}\theta'' - C1\,\emptyset = 0. \tag{20}$$

The transformed boundary conditions are

$$\eta = 0, \quad f = 0, \; \theta = 1, \quad \emptyset = 1,$$
$$\eta \longrightarrow \infty, \; f' = 0, \; \theta = 0, \quad \emptyset = 0, \tag{21}$$

where prime denotes differentiation with respect to η, and the key thermophysical parameters dictating the flow dynamics are defined by

$$Nr = \frac{(\rho_p - \rho_{f\infty})(\phi_w - \phi_\infty)}{\rho_{f\infty}\beta(T_w - T_\infty)(1 - \phi_\infty)}, \; Nb = \frac{\varepsilon\beta(\rho c)_p D_B(\phi_w - \phi_\infty)}{(\rho c)_f \alpha_m}, Nt = \frac{\varepsilon(\rho c)_p D_T(T_w - T_\infty)}{(\rho c)_f \alpha_m T_\infty}$$
$$Le = \frac{\alpha_m}{\varepsilon D_B},$$

$$Nv = -\frac{1}{\gamma(\phi_w - \phi_\infty)}, M = \frac{\sigma\beta_0{}^2 x}{\rho Ra_x{}^{1/2}}, \quad R = \frac{16T_\infty{}^3\sigma^*}{3K^*k}, \quad Cr = \frac{k_0 x^2}{D_B Ra_x}.$$

Other quantities of practical interest in this problem are local Nusselt number (Nu_x) and the local Sherwood number (Sh_x),which are defined as

$$Nu_x = \frac{xq_w}{k_m(T_w - T_\infty)}, \quad Sh_x = \frac{xJ_w}{D_B(\phi_w - \phi_\infty)}, \tag{22}$$

where, q_w is the wall heat flux and J_w is the wall mass flux. The set of ordinary differential equations (18) – (20) are highly non-linear, and therefore cannot be solved analytically. The finite-element method [36, 37, 38, 39] has been implemented to solve these non-linear equations.

III. NUMERICAL PROCEDURE

3.1. The finite-element method

The Finite-element method (FEM) is such a powerful method for solving ordinary differential equations and partial differential equations. The basic idea of this method is dividing the whole domain into smaller elements of finite dimensions called finite elements. This method is such a good numerical method in modern engineering analysis, and it can be applied for solving integral equations including heat transfer, fluid mechanics, chemical processing, electrical systems, and many other fields. The procedure involved in the Finite-element method is as follows.

3.2. Variational formulation

The variational form related with Eqs. (18) to (20) over a typical linear element (η_e, η_{e+1}) is given by

$$\int_{\eta_e}^{\eta_{e+1}} w_1\left(\frac{Nv}{(Nv - \emptyset)}f''' + \frac{Nv}{(Nv - \emptyset)^2}f'\emptyset' - (\theta' - Nr\,\emptyset') - Mf'\right)d\eta = 0 \tag{23}$$

$$\int_{\eta_e}^{\eta_{e+1}} w_2\left((1 + R)\theta'' + Nc\,\emptyset\,\theta'' + \tfrac{3}{2}f\theta' + Nc\,\theta'\emptyset' + Nt(\theta')^2 + Nb\,\emptyset'\theta'\right)d\eta = 0 \tag{24}$$

$$\int_{\eta_e}^{\eta_{e+1}} w_3\left(\emptyset'' + \frac{3}{2}Le\, f\,\emptyset' + \frac{Nt}{Nb}\theta'' - C1\,\emptyset\right)d\eta = 0 \tag{25}$$

where w_1, w_2, and w_3 are weighted functions and may be regarded as the variations in f, θ, and $\emptyset$, respectively.

3.3. Finite- element formulation

The finite-element form may be attained from above equations by replacing finite-element approximations of the form

$$f = \sum_{j=1}^{3} f_j \psi_j \ , \theta = \sum_{j=1}^{3} \theta_j \psi_j \ , \ \emptyset = \sum_{j=1}^{3} \emptyset_j \psi_j \qquad (26)$$

with $w_1 = w_2 = w_3 = \psi_i, \qquad (i = 1,2,3).$

where ψ_i are the shape functions for a typical element

(η_e, η_{e+1}) and are defined as

$$\psi_1^e = \frac{(\eta_{e+1}+\eta_e-2\,\eta)\,(\eta_{e+1}-\eta)}{(\eta_{e+1}-\eta)^2},$$

$$\psi_2^e = \frac{4(\eta-\eta_e)(\eta_{e+1}-\eta)}{(\eta_{e+1}-\eta)^2},$$

$$\psi_3^e = \frac{(\eta_{e+1}+\eta_e-2\,\eta)\,(\eta-\eta_e)}{(\eta_{e+1}-\eta)^2},$$

$$\eta_e \le \eta \le \eta_{e+1}. \qquad (27)$$

The finite element model of the equations thus formed is given by

$$\begin{bmatrix} [K^{11}] & [K^{12}] & [K^{13}] \\ [K^{21}] & [K^{22}] & [K^{23}] \\ [K^{31}] & [K^{32}] & [K^{33}] \end{bmatrix} \begin{bmatrix} f \\ \theta \\ \emptyset \end{bmatrix} = \begin{bmatrix} \{r^1\} \\ \{r^2\} \\ \{r^3\} \end{bmatrix}$$

where $[K^{mn}]$ and $[r^m]$ $(m, n = 1, 2, 3)$ are defined as

$$K_{ij}^{\ 11} = -\frac{Nv}{(Nv-\emptyset)}\int_{\eta_e}^{\eta_{e+1}} \frac{\partial\psi_i}{\partial\eta}\frac{\partial\psi_j}{\partial\eta}\,d\eta + \frac{Nv}{(Nv-\emptyset)^2}\overline{f_1}\int_{\eta_e}^{\eta_{e+1}} \psi_i\psi_1\frac{\partial\psi_j}{\partial\eta}\,d\eta + \frac{Nv}{(Nv-\emptyset)^2}\overline{f_2}'\int_{\eta_e}^{\eta_{e+1}} \psi_i\psi_2\frac{\partial\psi_j}{\partial\eta}\,d\eta - M\int_{\eta_e}^{\eta_{e+1}} \psi_i\frac{\partial\psi_j}{\partial\eta}\,d\eta,$$

$$K_{ij}^{\ 12} = \int_{\eta_e}^{\eta_{e+1}} \psi_i\frac{\partial\psi_j}{\partial\eta}\,d\eta. \qquad K_{ij}^{\ 13} = -Nr\int_{\eta_e}^{\eta_{e+1}} \psi_i\frac{\partial\psi_j}{\partial\eta}\,d\eta$$

$$K_{ij}^{\ 21} = 0,$$

$$K_{ij}^{\ 22} = (1+R)\int_{\eta_e}^{\eta_{e+1}} \frac{\partial\psi_i}{\partial\eta}\frac{\partial\psi_j}{\partial\eta}\,d\eta + \frac{3}{2}\overline{f_1}\int_{\eta_e}^{\eta_{e+1}} \psi_i\psi_1\frac{\partial\psi_j}{\partial\eta}\,d\eta + \frac{3}{2}\overline{f_2}\int_{\eta_e}^{\eta_{e+1}} \psi_i\psi_2\frac{\partial\psi_j}{\partial\eta}\,d\eta + Nt\int_{\eta_e}^{\eta_{e+1}} \psi_i\left(\frac{\partial\psi_j}{\partial\eta}\right)^2 d\eta + Nc\overline{\emptyset_1}\int_{\eta_e}^{\eta_{e+1}} \psi_i\psi_1\frac{\partial\psi_j}{\partial\eta}\,d\eta + Nc\overline{\emptyset_2}\int_{\eta_e}^{\eta_{e+1}} \psi_i\psi_2\frac{\partial\psi_j}{\partial\eta}\,d\eta,$$

$$K_{ij}^{\ 23} = (Nc+Nb)\overline{\theta'}_1\int_{\eta_e}^{\eta_{e+1}} \psi_i\psi_1\frac{\partial\psi_j}{\partial\eta}\,d\eta + (Nc+Nb)\overline{\theta'}_2\int_{\eta_e}^{\eta_{e+1}} \psi_i\psi_2\frac{\partial\psi_j}{\partial\eta}\,d\eta,$$

$$K_{ij}^{\ 31} = 0,\ K_{ij}^{\ 32} = \frac{Nt}{Nb}\int_{\eta_e}^{\eta_{e+1}} \frac{\partial\psi_i}{\partial\eta}\frac{\partial\psi_j}{\partial\eta}\,d\eta,$$

$$K_{ij}^{\ 33} = \int_{\eta_e}^{\eta_{e+1}} \frac{\partial\psi_i}{\partial\eta}\frac{\partial\psi_j}{\partial\eta}\,d\eta + \frac{3}{2}Le\overline{f_1}\int_{\eta_e}^{\eta_{e+1}} \psi_i\psi_1\frac{\partial\psi_j}{\partial\eta}\,d\eta + \frac{3}{2}Le\overline{f_2}\int_{\eta_e}^{\eta_{e+1}} \psi_i\psi_2\frac{\partial\psi_j}{\partial\eta}\,d\eta - C1\int_{\eta_e}^{\eta_{e+1}} \psi_i\psi_j\,d\eta$$

$$r_i^1 = 0,\ r_i^2 = -\left(\psi_i\frac{d\psi_i}{d\eta}\right)_{\eta_e}^{\eta_{e+1}},\ r_i^3 = -\left(\psi_i\frac{d\theta}{d\eta} + \frac{d\varphi}{d\eta}\right)_{\eta_e}^{\eta_{e+1}}.$$

where , $\bar{f} = \sum_{j=1}^{3} f_i\frac{\partial\psi_i}{\partial\eta} \qquad \bar{\theta} = \sum_{j=1}^{3} \theta_i\frac{\partial\psi_i}{\partial\eta}, \qquad \bar{\varphi} = \sum_{j=1}^{3} \varphi_i\frac{\partial\psi_i}{\partial\eta}.$

After assembly of element equations, we get the system of strongly non-linear equations and are solved using a robust iterative scheme. The system is linearized by incorporating the functions $\bar{f}$, $\bar{\theta}$ and $\bar{\phi}$, which are assumed to be known. After imposing the boundary conditions, we get the less number of non-linear equations and are solved using Gauss elimination method.

IV. RESULTS AND DISCUSSION

Computational results depicting the effects of various thermophysical parameters on the nanofluid velocity, temperature, nanoparticle volume fraction, as well as the skin friction, local Nusselt and Sherwood number are obtained and displayed graphically in Figs. 2-19 and in tabular form in table 2. To validate our numerical results, we have compared a special case of our results with that of Noghrehabadi et al. [30] in table 1. The comparison shows good agreement and we are confident that our numerical method is accurate.

The impact of magnetic parameter (M) on velocity (f'), temperature (θ) and concentration of nanoparticle $(\emptyset)$ profiles are illustrated in Figs. 2 – 4. It is observed that, the velocity profiles decelerate, whereas, temperature distributions heighten in the boundary layer regime with increment in magnetic parameter (M). As the values of magnetic parameter (M) rises, the thickness of the solutal boundary layer elevates in the fluid region (Fig.4).

The velocity, temperature and nanoparticle volume fraction profiles for different values of variable viscosity parameter (Nv) are plotted in Figs. 5 – 7. It is clearly noticed from Fig.5 that the velocity profiles are highly influenced by the variable viscosity parameter (Nv) in the vicinity of the cone surface. But, in the areas far away from the cone surface, inside the boundary layer, the velocity profiles are poorly affected by (Nv). This is because of the reality that higher the values of (Nv) would increase the buoyancy force in the vicinity of the cone surface leads to increase the thickness of hydrodynamic boundary layer. The temperature distributions are elevated in the boundary layer region (Fig. 6) with the rising values of variable viscosity parameter (Nv). It is noted from Fig. 7 that the nanoparticle concentration distributions are deteriorated significantly from the surface of the cone into the boundary layer as the values of (Nv) increased. This is because of the reality that increasing variable viscosity parameter leads to decrease the concentration of nanoparticles.

Figs. 8 and 9 illustrate the influence of variable thermal conductivity parameter (Nc) on thermal and solutal boundary layers. An increase in the values of variable thermal conductivity parameter (Nc) elevates the magnitude of temperature distributions (Fig. 8). This is because of the fact that the thermal conductivity raises near surface of the cone as the values of variable thermal conductivity parameter (Nc) increases. However, the thickness of the solutal boundary layer decelerates near the cone surface with the improving values of (Nc).

The non-dimensional profiles of temperature and concentration of nanoparticles are displayed in Figs. 10 and

11 for various values of radiation parameter (*R*). With the higher values of (*R*) the temperature of the fluid rises in the boundary layer regime. This is because of the fact that imposing thermal radiation into the flow warmer the fluid, which causes an increment in the thickness of thermal boundary layer in the entire flow region (Fig.10). However, the concentration boundary layer thickness is deteriorated with increasing values of *R*.

Figures 12 and 13 depict the temperature (θ) and concentration (Ø) distributions for various values of thermophoretic parameter (*Nt*).Both the temperature and concentration profiles elevate in the boundary layer region for the higher values of thermophoretic parameter (*Nt*). Because of temperature gradient the thermophoretic force was developed in the boundary layer region and this force involves in the diffusion of nanoparticles from higher temperature region to the lower temperature region, causes the enhancement in the thickness of both thermal and concentration boundary layers.

Figures 14 – 15 shows the influence of Brownian motion parameter (*Nb*) on thermal and solutal boundary layer thickness. Brownian motion is the arbitrary motion of suspended nanoparticles in the base fluid and is more influenced by its fast moving atoms or molecules in the base fluid. It is worth to mention that Brownian motion is related to the size of nanoparticles and are often in the form of agglomerates and/or aggregates. It is noticed that, with the increasing values of Brownian motion parameter (*Nb*) the temperature of the fluid is elevated in the boundary layer regime (Fig.14). However, the concentration profiles are decelerated in the fluid regime as the values of (*Nb*) increases (Fig.15). Clearly, we noticed that Brownian motion parameter has significant influence on both temperature and concentration profiles.

The influence of Lewis number (*Le*) on temperature and concentration evolutions is plotted in Figs. 16 and 17.It is observed that both the temperature and concentration distributions decelerate with the increasing values of the Lewis number in the entire boundary layer region. By definition, the Lewis number represents the ratio of thermal diffusivity to the mass diffusivity. Increasing the Lewis number means a higher thermal diffusivity and a lower mass diffusivity, and this produces thinner thermal and concentration boundary layers.

The temperature and concentration profiles are depicted in Figs. 18 – 19 for diverse values of chemical reaction parameter (*Cr*). It is noticed from Fig.18 that the temperature profiles of the fluid decelerated in the entire boundary layer regime with the higher values of chemical reaction parameter (*Cr*). The concentration profiles are highly influenced by the chemical reaction parameter. Chemical reaction parameter (*Cr*) increases means lesser the molecular diffusivity, as the result thinner the solutal boundary layer thickness (Fig.19).

The values of Nusselt number $-\theta'(0)$ and Sherwood number $-\emptyset'(0)$ are calculated for diverse values of the key parameters entered into the problem when the cone surface is hot and the results are shown in Table 2. The values of Nusselt and Sherwood number are both diminish as magnetic parameter (*M*) rises. Magnitude of the both heat and mass transfer rates is amplified in the fluid regime as the values of (*Nv*) increases. The non-dimensional heat transfer rates depreciate whereas non-dimensional mass transfer rate escalates with the higher values of variable thermal conductivity parameter (*Nc*). The impact of thermophoresis parameter (*Nt*) on $-\theta'(0)$ and $-\emptyset'(0)$ is also presented in table 2. It is evident that the non-dimensional rates of heat and mass transfer are both deteriorate with the higher values of (*Nt*). It is also seen from this table that Nusselt number values decelerates, whereas Sherwood number values enhances in the fluid region as the values of Brownian motion parameter (*Nb*) rises. Higher the values of chemical reaction parameter (*Cr*) intensify the non-dimensionless heat and mass transfer rates.

V. CONCLUSIONS

MHD natural convection boundary layer flow, heat and mass transfer characteristics over a vertical cone embedded in a porous medium saturated by a nanofluid under the impact of variable viscosity, variable thermal conductivity, thermal radiation and chemical reaction is investigated in this research. The two significant effects of nanoparticles, Brownian motion and thermophoresis are considered into the account. The hydrodynamic, thermal and solutal boundary layers thickness were analyzed for various values of the pertinent parameters and the results are shown in figures. Furthermore, the impact of these parameters on Nusselt number and Sherwood number are also calculated. The important findings of the present study are summarized as follows.

a) The velocity and temperature distributions are heightens whereas the nanoparticle volume fraction concentration profiles decelerate in the boundary layer region as the values of variable viscosity parameter (*Nv*) increases.
b) Increasing values of (*Nc*) elevates the thickness of thermal boundary layer. However, solutal boundary layer thickness deteriorates with the rising values of (*Nc*).
c) Increasing the values of variable viscosity parameter (*Nv*) raises the dimensionless rates of heat and mass transfer.
d) As the values of variable thermal conductivity parameter (*Nc*) increases the local Nusselt number values decreases whereas the values of local Sherwood number escalates in the fluid region.

e) Both the temperature and concentration profiles elevates in the boundary layer regime as the values of (*Nt*) increases.
f) With increase in the values (*Nb*) upsurges the temperature of the fluid, however, it deteriorates the volume fraction concentration of nanoparticles.
g) Increase of chemical reaction parameter (*Cr*) depreciates the thickness of the solutal boundary layer.

Table 1. Comparison of $-\theta'(0)$ with previously published work with fixed values of
$Nt = 10^{-6}, Nb = 10^{-5}, Nr = 10^{-3}, Nc = 0.$

Parameter		Noghrehabadi et al.[30]	Present Study
Nv	*Le*	$-\theta'(0)$	$-\theta'(0)$
2.0	1000	0.7584	0.7591
10.0	1000	0.7670	0.7675
20.0	1000	0.7680	0.7686
200.0	1000	0.7688	0.7694

Table 2. The values of Nusselt number ($-\theta'(0)$) and Sherwood number ($-\phi'(0)$) for different values of *M*, *Nv*, *Nc*, *Nt*, *Nb*, *Cr*.

M	Nv	Nc	Nt	Nb	Cr	$-\theta'(0)$	$-\phi'(0)$
0.1	3.0	0.1	0.5	0.5	0.1	0.324188	1.101870
0.4	3.0	0.1	0.5	0.5	0.1	0.313384	1.073523
0.7	3.0	0.1	0.5	0.5	0.1	0.300097	1.038980
1.0	3.0	0.1	0.5	0.5	0.1	0.287081	1.005489
0.5	2.0	0.1	0.5	0.5	0.1	0.250541	0.954590
0.5	10.0	0.1	0.5	0.5	0.1	0.280877	1.046247
0.5	50.0	0.1	0.5	0.5	0.1	0.298977	1.102604
0.5	100	0.1	0.5	0.5	0.1	0.318760	1.165578
0.5	3.0	0.1	0.5	0.5	0.1	0.298977	1.102604
0.5	3.0	0.5	0.5	0.5	0.1	0.260772	1.143616
0.5	3.0	1.0	0.5	0.5	0.1	0.227301	1.178045
0.5	3.0	1.5	0.5	0.5	0.1	0.202978	1.201918
0.5	3.0	0.1	0.1	0.5	0.1	0.381519	1.105337
0.5	3.0	0.1	0.2	0.5	0.1	0.359939	1.087014
0.5	3.0	0.1	0.3	0.5	0.1	0.338796	1.076160
0.5	3.0	0.1	0.4	0.5	0.1	0.319463	1.073046
0.5	3.0	0.1	0.5	0.5	0.1	0.298977	1.102604
0.5	3.0	0.1	0.5	0.8	0.1	0.253957	1.149124
0.5	3.0	0.1	0.5	1.2	0.1	0.199689	1.177921
0.5	3.0	0.1	0.5	1.6	0.1	0.154740	1.193862
0.5	3.0	0.1	0.5	0.5	0.1	0.289212	0.846373
0.5	3.0	0.1	0.5	0.5	0.2	0.295030	0.981077
0.5	3.0	0.1	0.5	0.5	0.3	0.298977	1.102604
0.5	3.0	0.1	0.5	0.5	0.4	0.301923	1.213673

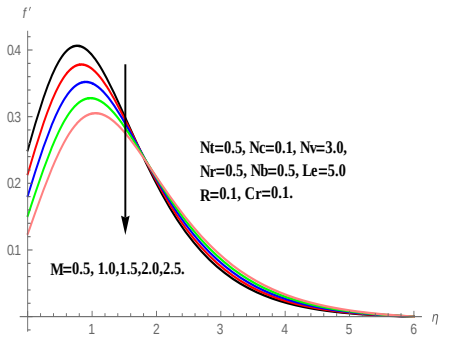

Fig.2.Velocity profiles for various values of (*M*)

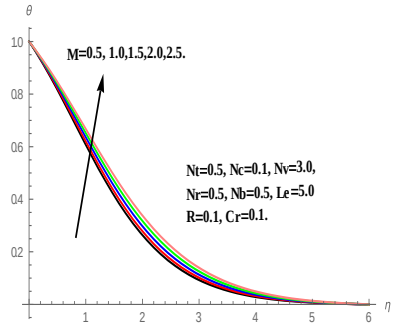

Fig.3.Temperature profiles for various values of (*M*)

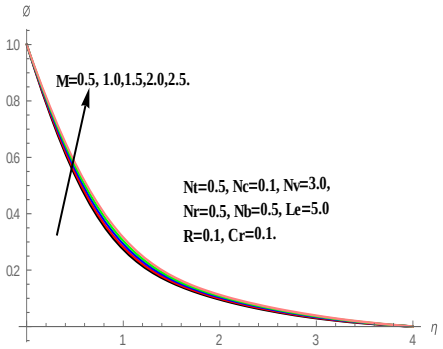

Fig.4.Concentration profiles for various values of (*M*)

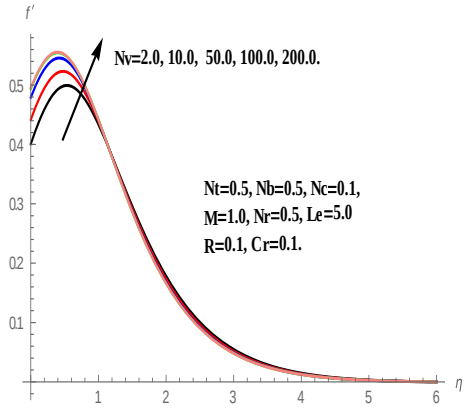

Fig.5.Velocity profiles for various values of (*Nv*)

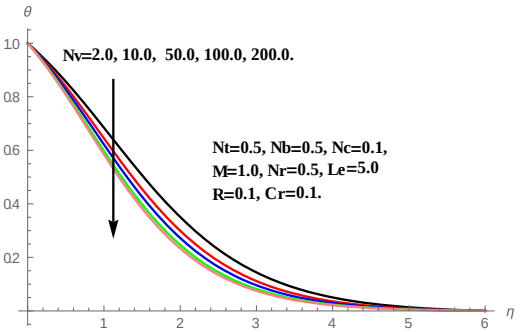

Fig.6.Temperature profiles for various values of (*Nv*)

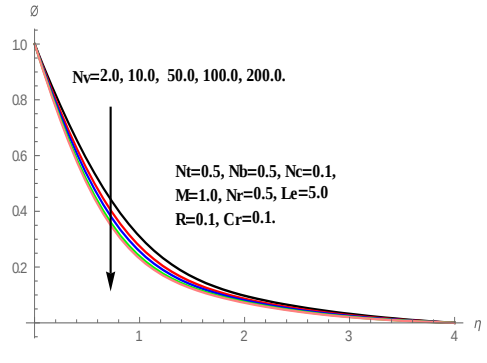

Fig.7.Concentration profiles for various values of (*Nv*)

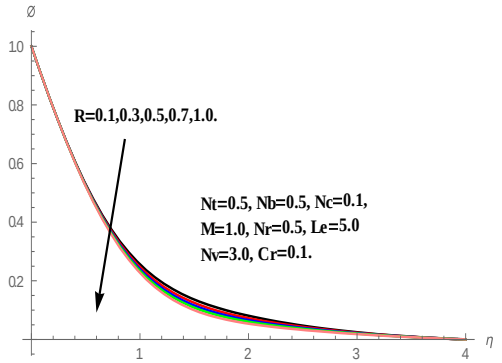

Fig.11.Concentration profiles for various values of (*R*)

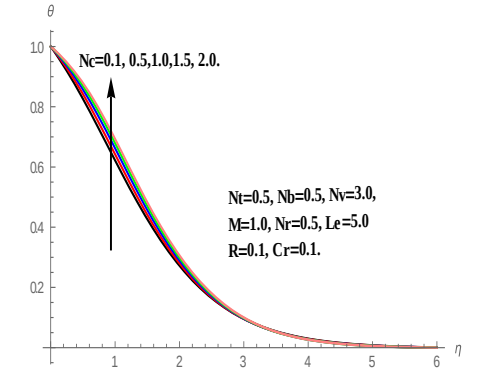

Fig.8.Temperature profiles for various values of (*Nc*)

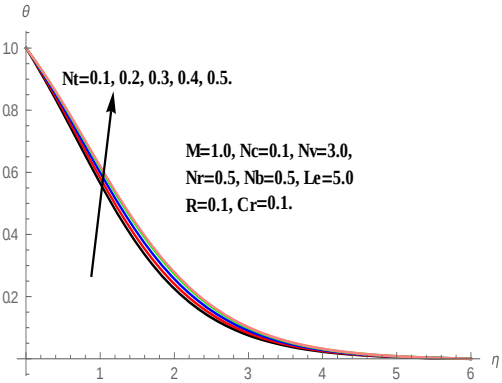

Fig.12.Temperature profiles for various values of (*Nt*)

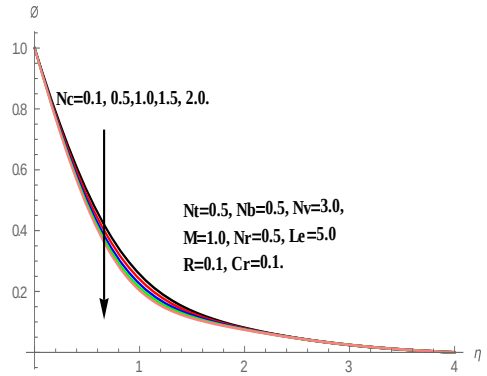

Fig.9.Concentration profiles for various values of (*Nc*)

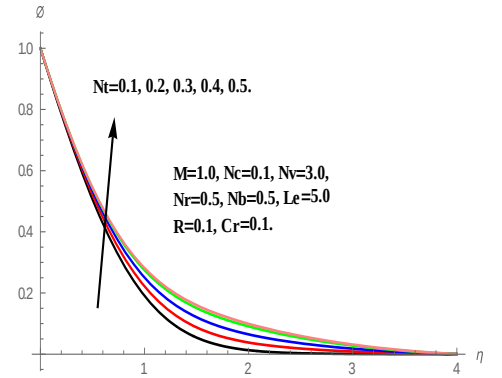

Fig.13.Concentration profiles for various values of (*Nt*)

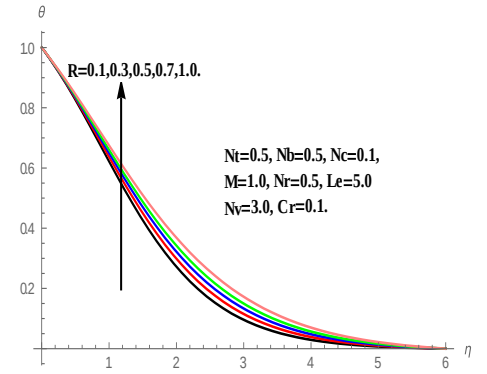

Fig.10.Temperature profiles for various values of (*R*)

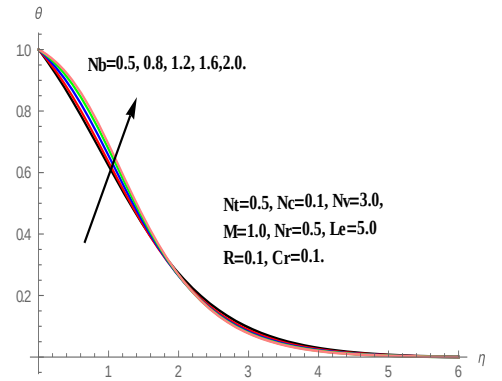

Fig.14.Temperature profiles for various values of (*Nb*)

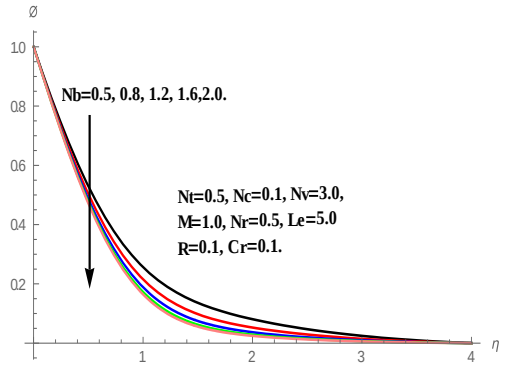

Fig.15.Concentration profiles for various values of (*Nb*)

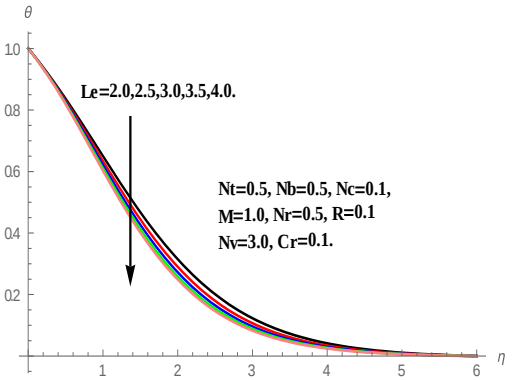

Fig.16.Temperature profiles for various values of (*Le*)

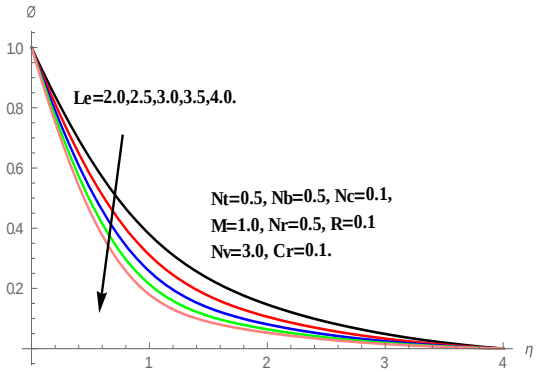

Fig.17.Concentration profiles for various values of (*Le*)

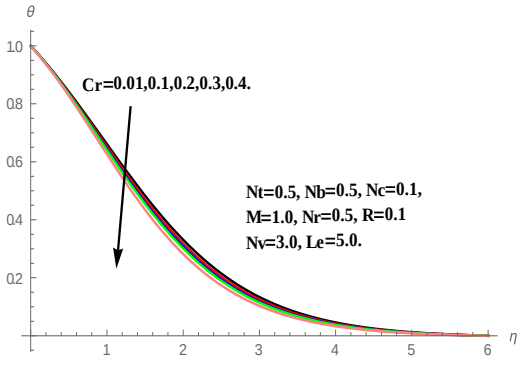

Fig.18.Temperature profiles for various values of (*Cr*)

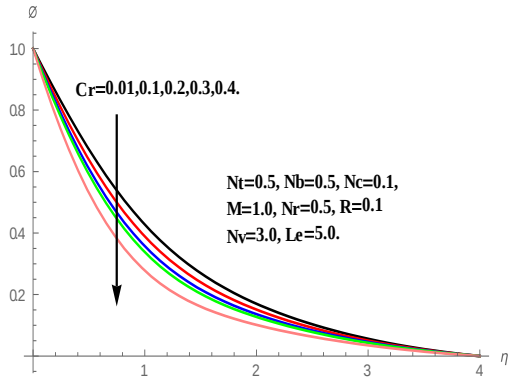

Fig.19.Concentration profiles for various values of (*Cr*)

REFERENCES

[1]. Choi SUS. Enhancing thermal conductivity of fluids with nanoparticles, developments and applications of non-Newtonian flows, in: D.A. Siginer, H.P. Wang (Eds.), FED-Vol. 231/MD, Vol. 66, The American Society of Mechanical Engineers (1995) 99–105.

[2]. Eastman JA, Choi SUS, Li S, Thompson LJ, Lee S. Enhanced thermal conductivity through the development of nanofluid, in: S. Komarneni, J.C. Parker, H.J. Wollenberger (Eds.), Nanophase and Nanocomposite Materials II, MRS, Pittsburg, PA (1997) 3–11.

[3]. Eastman JA, Choi SUS, Li S, Yu W, Thompson LJ. Anomalously increased effective thermal conductivities of ethylene glycol-based nano-fluids containing copper nano-particles. Appl.Phys. Lett. 78 (2001) 718–720.

[4]. Xuan Y, Li Q, Investigation on Convective Heat Transfer and Flow Features of Nanofluids, ASME J. Heat Transfer, 125 (2003) 151–155.

[5]. Buongiorno J. Convective transport in nanofluids. ASME J. Heat Transfer 128 (2006) 240–250.

[6]. Nield DA, Kuznetsov AV, The Cheng - Minkowycz problem for natural convection boundary-layer flow in a porous medium saturated by a nanofluid. Int. J. Heat Mass Transfer 52 (2009) 5792–5795

[7]. Kuznetsov AV, Nield DA, Natural convection boundary-layer of a nanofluid past a vertical plate. Int. J. Therm. Sci 49 (2010) 243–247.

[8]. Chamkha. A.J, Rashad. A.M, Unsteady Heat and Mass Transfer by MHD Mixed Convection Flow from a Rotating Vertical Cone with Chemical Reaction and Soret and Dufour Effects. The Canadian Journal of Chemical Engineering 92 (2014) 758-767.

[9]. Chamkha. A.J, Abbasbandy. S, Rashad. A. M, Vajravelu. K, Radiation effects on mixed convection about a cone embedded in a porous medium filled with a nanofluid, Meccanica 48 (2013) 275-285.

[10]. Gorla. R.S.R, Chamkha. A.J, Ghodeswar. V, Natural convective boundary layer flow over a vertical cone embedded in a porous medium saturated with a nanofluid, Journal of Nanofluids 3 (2014) 65-71.

[11]. Chamkha. A. J, Abbasbandy. S, Rashad. A. M, Non-Darcy natural convection flow of non-Newtonian nanofluid over a cone saturated in a porous medium with uniform heat and volume fraction fluxes, International Journal of Numerical Methods for Heat and Fluid Flow 25 (2015) 422-437.

[12]. Cheng. C.Y, Double-diffusive natural convection from a vertical cone in a porous medium saturated with a nanofluid, J. Chinese Soc. Mech. Engrs. 34 (2013) 401-409.

[13]. Behseresht. A, Nogrehabadi. A, Ghalambaz. M, Natural-convection heat and mass transfer from a vertical cone in porous media filled with nanofluids using practical ranges of nanofluids

thermo-physical properties, Chem. Engnrg. Res. Design 92 (2014) 447-452.
[14]. Ghalambaz. M, Behseresht. A, Behseresht. A, Chamkha. A.J, Effect of nanoparticle diameter and concentration on natural convection in Al_2O_3 -water nanofluids considering variable thermal conductivity around a vertical cone in porous media, Adv. Powder Technology 26 (2015) 224-235.
[15]. Noghrehabadi. A, Behseresht. A, Ghalambaz. M, Natural convection of nanofluid over vertical plate embedded in porous medium: prescribed surface heat flux, Applied Mathematics and Mechanics 34 (2013) 669-686.
[16]. Noghrehabadi. A, Pourrajab. R, Ghalambaz. M, Effect of partial slip boundary condition on the flow and heat transfer of nanofluids past stretching sheet prescribed constant wall temperature, International Journal of Thermal Sciences 54 (2013) 253-261
[17]. Noghrehabadi. A, Saffarian. M. R, Pourrajab. R, Ghalambaz. M, Entropy analysis for nanofluid flow over a stretching sheet in the presence of heat generation/absorption and partial slip, Journal of Mechanical Science and Technology 27 (2013) 927-937.
[18]. Teamah. M. A, El-Maghlany. W. M, Augmentation of natural convection heat transfer in square cavity by utilizing nanofluids in the presences of magnetic field and heat source, International Journal of Thermal Sciences 58 (2012) 130-142.
[19]. Sudarsana Reddy. P, Suryanarayana Rao. K. V, MHD natural convection heat and mass transfer of Al_2O_3 - water and Ag - water nanofluids over a vertical cone with chemical reaction, Procedia Engineering 127 (2015) 476 – 484.
[20]. Sheremet. M.A., and Pop, I., Conjugate natural convection in a square porous cavity filled by a nanofluid using Buongiorno's mathematical model, Int. J. Heat Mass Transfer, Vol. 79, (2014) 137-145.
[21]. Sheremet, M.A., Pop, I., and Rahman, M.M., Three-dimensional natural convection in a porous enclosure filled with a nanofluid using Buongiorno's mathematical model, Int. J. Heat Mass Transfer, vol. 82, (2015) 396-405
[22]. Ellahi, R., Aziz, S., and Zeeshan, A., Non Newtonian nanofluids flow through a porous medium between two coaxial cylinders with heat transfer and variable viscosity, Journal of Porous Media, Vol. **16 (3)**, (2013) 205-216.
[23]. Sheikholeslami, M., Ellahi, R., Mohsan Hassan., and Soheil Soleimani, A study of natural convection heat transfer in a nanofluid filled enclosure with elliptic inner cylinder, International Journal of Numerical Methods for Heat & Fluid Flow, Vol. 24, (2014)1906 – 1927.
[24]. Chaim TC. Heat transfer with variable thermal conductivity in a stagnation point flow towards a stretching sheet. Int Commun Heat Mass Transfer 23, (1996) 239–248.
[25]. Oztop HF, Abu-Nada E. Numerical study of natural convection in partially heated rectangular enclosures filled with nanofluids. Int J Heat Mass Transfer 29, (2008) 1326–1336.
[26]. Das SK, Choi SUS, Yu W, Pradeep T. Nanofluids – science and technology. Hoboken: John Wiley & Sons Publishers; 2007.
[27]. Chandrasekar M, Suresh S. A review on the mechanisms of heat transport in nanofluids. Heat Transfer Eng 30 (2009) 1136–1150.
[28]. Khanafer K, Vafai K. A critical synthesis of thermophysical characteristics of nanofluids. Int J Heat Mass Transfer 54 (2011) 4410–28.
[29]. Kakaç S, Pramuanjaroenkij A. Review of convective heat transfer enhancement with nanofluids. Int J Heat Mass Transfer 52 (2009) 3187–3196.
[30]. Noghrehabadi. A, Behseresht. A, Flow and heat transfer affected by variable properties of nanofluids in natural-convection over a vertical cone in porous media, Comput. Fluids 88 (2013) 313–325
[31]. P. Sudarsana Reddy, Ali J. Chamkha, Influence of size, shape, type of nanoparticles, type and temperature of the base fluid on natural convection MHD of nanofluids, Alexandria Eng. J., 55 (2016) 331-341.
[32]. P. Sudarsana Reddy, P. Sreedevi, Ali J. Chamkha, MHD boundary layer flow, heat and mass transfer analysis over a rotating disk through porous medium saturated by Cu-water and Ag-water nanofluid with chemical reaction, Powder Technology 307 (2017), 46 – 55.
[33]. Abdelraheem M. Aly, Natural convection over circular cylinders in a porous enclosure filled with a nanofluid under thermo-diffusion effects, Journal of the Taiwan Institute of Chemical Engineers 70 (2017) 88–103.
[34]. Yan Zhang, Min Zhang, Yu Bai, Unsteady flow and heat transfer of power-law nanofluid thin film over a stretching sheet with variable magnetic field and power-law velocity slip effect, Journal of the Taiwan Institute of Chemical Engineers 70 (2017) 104–110.
[35]. Dhanai R , Rana P, Kumar L . Critical values in slip flow and heat transfer analysis of non-Newtonian nanofluid utilizing heat source/sink and variable magnetic field: Multiple solutions. J Taiwan Inst Chem Eng 2016; 58: 155–164.
[36]. Anwar Bég, O., Takhar, H. S., Bhargava, R., Rawat, S., and Prasad, V.R., Numerical study of heat transfer of a third grade viscoelastic fluid in non-Darcian porous media with thermophysical effects, Phys. Scr., 77 (2008) 1–11.
[37]. Sudarsana Reddy, P and Chamkha, AJ, Soret and Dufour effects on MHD heat and mass transfer flow of a micropolar fluid with thermophoresis particle deposition, Journal of Naval Architechure and Marine Engineering, 13 (2016) 39-50.
[38]. Rana, P., and Bhargava, R., Flow and heat transfer of a nanofluid over a nonlinearly stretching sheet: a numerical study, Comm. Nonlinear Sci. Numer. Simulat.,17 (2012) 212–226.
[39]. Sudarsana Reddy, P and Chamkha, A.J., Soret and Dufour effects on MHD convective flow of Al_2O_3–water and TiO_2–water nanofluids past a stretching sheet in porous media with heat generation/absorption, Advanced Powder Technology 27 (2016) 1207 – 1218.